Effects of ballistic atom movements on ordering transitions of binary alloys

L. B. Hong and B. Fultz
Division of Engineering and Applied Science, California Institute of Technology, 138-78, Pasadena, California 91125
(Received 29 August 1994)

We studied chemical order-disorder transitions in equiatomic alloys on a square lattice in the presence of both thermal and ballistic atom movements. Using Monte Carlo simulations with a vacancy mechanism, we determined the steady states of the alloys for various combinations of f (fraction of ballistic atom movements) and T (temperature), and located the order-disorder phase boundary on a diagram of T vs f. For symmetric interatomic potentials, the dynamical critical temperature decreased with f as $(1-1.58f)$ when $f \leq 0.36$, and decreased rapidly with f when $0.36 < f \leq 0.43$. No ordered phase was stable at any temperature when f was greater than a critical value of $f_c^0 > 0.43$. An Onsager-type kinetic rate equation was modified to include ballistic atom movements, and was used to identify two reasons why the ballistic atom movements suppress the dynamical critical temperature: (1) the ballistic atom movements dilute the enthalpy driving force for ordering, and (2) at low temperatures the ratio of thermal mobility coefficient to ballistic mobility coefficient becomes small.

I. INTRODUCTION

High-energy ball milling[1] and high-energy ion bombardment[2] are popular methods for synthesizing alloys in states far from thermodynamic equilibrium. In these energetic processes, some atom movements occur athermally in response to defects generated by the milling process or by nuclear collisions. Atoms in these "driven" alloys are forced out of local environments characteristic of their thermodynamic distribution. Acting in parallel are the usual thermal movements, which tend to restore these thermodynamic environments. Because both kinetic processes are Markovian, a steady state will be achieved eventually.[3] This steady state is termed a "dynamical steady state" to distinguish it from the steady state of thermodynamic equilibrium.

To model these dynamical phenomena, Martin and co-workers proposed a model of driven systems that is amenable to study by analytical methods and computer simulations.[4–11] In this model, the ballistic atom movements are assumed to occur at random, while the thermal atom movements follow conventional activated state rate theory. Much work was devoted to constructing and elucidating the properties of a "stochastic potential," which is the analogy for a driven alloy of the free energy for a thermodynamic alloy.[4–10] This stochastic potential is sensitive to features of the kinetic mechanism; a dependence of the dynamical critical temperature on the details of replacement collision sequences was found previously.[5,9] The stochastic potential is also sensitive to the nature of the approximations (point or pair, for example) used in the analytical theory, however.

In the present study, we used Monte Carlo simulations with a vacancy mechanism for both the thermal and ballistic atom movements. The vacancy mechanism provides a richness of kinetic features that are not available with the pair interchange mechanism, and offers new ways by which the mechanism of atoms movements can affect the dynamical steady state of the alloy.[9] Especially at low temperature, however, the vacancy mechanism exhibits subleties of behavior that cannot be included in analytical theories based on approximations with small cluster variables. The present work examined how the strong diffusional correlation factors unique to the vacancy mechanism[12–17] affect the phase boundary between ordered and disordered phases at various temperatures, T, and fraction of ballistic atom movements, f. Our results suggest a simple but general picture of how the shape of a dynamical phase boundary can be affected by a combination of thermodynamic and kinetic effects.

II. MONTE CARLO SIMULATIONS

Monte Carlo simulations were performed with equiatomic alloys on a square lattice with periodic boundaries. The typical lattice had $N=256\times256=65\,536$ sites, but larger lattices of 262 144 sites were also used. We included only first-nearest-neighbor (1nn) pairwise interactions between the two species of atoms, A and B. The 1nn M-N ($M,N = A$ or B) pair potential is denoted by V_{MN} (its units are kT). The 1nn pairwise exchange potential V is defined as

$$V \equiv (V_{AA} + V_{BB} - 2V_{AB})/2 \ . \tag{1}$$

For all results reported here, we fixed $V_{AB}=0$. We also used $V_{AA}=V_{BB}>0$ (so $V=V_{AA}=V_{BB}$), unless otherwise specified. The pairwise exchange potential, V, sets the thermodynamic critical temperature T_c^0. For thermodynamic alloys without ballistic atom movements ($f=0$), it is known that[18]

$$T_c^0 = \frac{V}{0.88} \tag{2}$$

exactly, or

$$T_c'^0 = \frac{V}{0.5} \tag{3}$$

in the mean-field Bragg-Williams approximation. It is the goal of this study to investigate how the critical temperature is altered by ballistic atom movements when $f \neq 0$.

Each kinetic step occurred with a vacancy mechanism algorithm,[14–16] modified to include ballistic atom movements. All sites of the lattice were occupied by A and B atoms, except for one site left unoccupied as a vacancy. An atom could move by exchanging its position with a neighboring vacancy. To include ballistic atom movements, a random number $\mathcal{R}$ was first chosen, where $0 \leq \mathcal{R} < 1$. If $\mathcal{R} < f$ (f is the fraction of ballistic atom movements), the atom movement was determined to be ballistic. If so, the vacancy had an equal probability of exchanging sites with any of its 1nn atoms, and one of the 1nn atoms was chosen at random. Otherwise the movement was a thermal movement, and every neighboring atom has its own thermal movement frequency ω_j. The thermal movement probabilities $\{p_j\}$ were set by the competition among all z 1nn atoms (z is the 1nn coordination number, equal to 4 for the square lattice):

$$p_j = \frac{\omega_j}{\sum_{j'=1}^{z} \omega_{j'}} . \tag{4}$$

Using these thermal atom movement probabilities $\{p_j\}$ as weights, the Monte Carlo algorithm then selected at random one of the neighboring atoms to exchange sites with the vacancy. The thermal movement frequencies $\{\omega_j\}$ were calculated with activated state rate theory:

$$\omega_j \propto \exp\left[\frac{E_j}{kT}\right] . \tag{5}$$

Here E_j is the initial bond energy for the jth neighboring atom:

$$E_J = N_{AA}V_{AA} + N_{BB}V_{BB} + N_{AB}V_{AB} , \tag{6}$$

with N_{MN} defined as the number of M-N bonds ($M,N = A$ or B) to the jth atom. Note that E_j [Eq. (6)], and therefore ω_j [Eq. (5)] and p_j [Eq. (4)], are dependent on the particular local environment of each atom.

All simulations started from an initially random arrangement of atoms (characteristic of a quench from $T = \infty$) unless otherwise specified. The simulated lattice was examined periodically to obtain Warren-Cowley short-range order (SRO) parameters $\{\alpha(r)\}$,[19] an average domain length scale $\langle r \rangle$ and the long-range order (LRO) parameter L. The SRO parameter $\alpha(1)$ was computed by counting the number of all 1nn A-B pairs N_{AB1}, and $\alpha(2)$ was obtained by counting the 2nn A-B pairs, N_{AB2}:

$$\alpha(1) = 1 - \frac{N_{AB1}}{N} , \tag{7a}$$

$$\alpha(2) = 1 - \frac{N_{AB2}}{N} , \tag{7b}$$

where $\alpha(1) = \alpha(2) = 0$ for the disordered state, and $\alpha(1) = -\alpha(2) = -1$ for perfect order. The LRO parameter, L, was obtained by a simulated x-ray-diffraction procedure,[20] which provided diffraction intensities $I(\mathbf{k})$ through two-dimensional Fourier transformation:

$$I(\mathbf{k}) = \left| \sum_{\text{all sites}} f_{\text{at}}(\mathbf{r}) \exp(-i\mathbf{k}\cdot\mathbf{r}) \right|^2 . \tag{8}$$

Here $f_{\text{at}}(\mathbf{r})$ is the atomic form factor for the atom at site $\mathbf{r}$, and $f_{\text{at}} = 1$ for A atoms and $f_{\text{at}} = 0$ for B atoms. The lowest order superlattice diffraction peak corresponding to the checkerboard ordered structure on a square lattice is $(\frac{1}{2}\frac{1}{2})$, while the lowest order fundamental peak is (1 0). The intensities of these peaks, $I_{\frac{1}{2}\frac{1}{2}}$, and I_{10}, were obtained by integrating $I(\mathbf{k})$ over a square around their centers in k space of edge length $2\pi/(16a)$ (a is the lattice constant of the square lattice). The LRO parameter L was then obtained from the intensities in the usual way:

$$L = \left[\frac{I_{\frac{1}{2}\frac{1}{2}}}{I_{10}} \right]^{1/2} , \tag{9}$$

where $0 \leq L \leq 1$, with 1 corresponding to perfect order.

To determine a characteristic length of the ordered domains, $\langle r \rangle$, we calculated a real-space autocorrelation function after the alloy was transformed as follows. First, an overlay mask for the perfect ordered structure was generated for all x and y coordinates (i and j, respectively) of the lattice. For $i+j$ even, each site in the mask was $+1$; for $i+j$ odd, the site was -1. The alloy itself was then transformed by first assigning a value of $+1$ to each alloy site occupied by an A atom, and -1 to each site occupied by a B atom. These numbers of ± 1 for all sites in the alloy were then multiplied by the numbers for their corresponding sites [same (i,j)] of the mask. This generated the transformed alloy. (For alloys having a strong domain structure, the different domains were seen in the transformed alloy as regions of sites with a preponderance of either $+1$ or -1.) The autocorrelation function of the transformed alloy, $A \otimes A$, was then calculated by the usual procedure:

$$A \otimes A(\mathbf{R}) = \sum_{i=1}^{256} \sum_{j=1}^{256} A(i,j) \times A(i+R_i, j+R_j) . \tag{10}$$

The autocorrelation function, $A \otimes A(\mathbf{R})$, was calculated for various magnitudes $|\mathbf{R}|$ (where $|\mathbf{R}| = \sqrt{R_i^2 + R_j^2}$), and then averaged over the x and y directions. We determined the zero crossing on graphs of the averaged $A \otimes A$ versus $|\mathbf{R}|$. This value of $|\mathbf{R}|$ at the zero crossing was defined as the characteristic length for the ordered alloy $\langle r \rangle$.

Our interest was in determining the steady states of the alloys, not their kinetic behavior. This required monitoring the state of order in the alloy during the simulation to ensure that L did not change if the simulation proceeded further, except for expected fluctuations. To ensure that the steady state was attained, we typically waited for times that were a factor of 10 longer than the time for which the steady-state value of L was first detected. In several cases we confirmed that the steady states were indeed correct by starting the simulations with the alloys having perfect ordered structures, and verifying that the

same order parameters were eventually attained as for the cases of initially disordered alloys. Finally, we note that our approach of fixing the fraction, f, may seem different from previous work that used a constant rate of ballistic jumps.[4–11] For example, the thermal jump rate depends on the state of order in the alloy, so a constant ballistic jump rate may be more appropriate for determining the kinetics of the alloy. For determining the steady states of a given alloy, however, both methods must provide the same result, since both L and f are constant in steady state, and are set by temperature and the ballistic jump rate. In particular, we expect the steady-state critical temperature to be the same with either approach.

III. MONTE CARLO RESULTS

We performed a series of Monte Carlo simulations with variable V and fixed f. Typical results are presented in Fig. 1. For the thermodynamic case with $f=0$, the critical temperature, T_c^0 was identified with the inflection point of the cure to be near $V/kT=0.88$, consistent with Eq. (2). There are many similarities between the L vs V curves for $f=0$ and for some cases of $f>0$, although the ballistic atom movements tend to disorder the alloy and suppress the critical temperature. The critical temperatures, T_c^f, were determined for $f>0$ either by identifying the inflection points of the L vs V curves, or by locating the points where L had the same value as at T_c^0 when $f=0$. Numbers obtained from both methods agreed well, and we do not distinguish them hereafter. On the other hand, the L vs V curve for $f=0.55$ has an almost flat and featureless shape, and is quite different from the curves for $f=0$, 0.2, and 0.35. When $f=0.55$, the largest value of L was no more than 0.2, even for temperatures as low as $V/kT=100$. Direct observations showed that the lattice had only small ordered domains and no long-range ordering. Evidently there is no ordering transition at any temperature when $f=0.55$.

We also performed a series of Monte Carlo simulations with variable f and fixed V. Figure 2 shows typical L vs f curves for different V. Qualitatively, the shapes of these curves are reminiscent of curves of L vs T. Again,

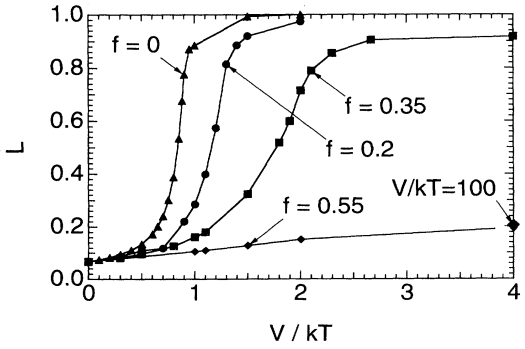

FIG. 1. The steady-state LRO parameter, L, as a function of V (i.e., inverse temperature) with $f=0$ (triangles), $f=0.2$ (circles), $f=0.35$ (squares), and $f=0.55$ (diamonds). The data point labeled with "$V/kT=100$" was for $f=0.55$ and $V=100$.

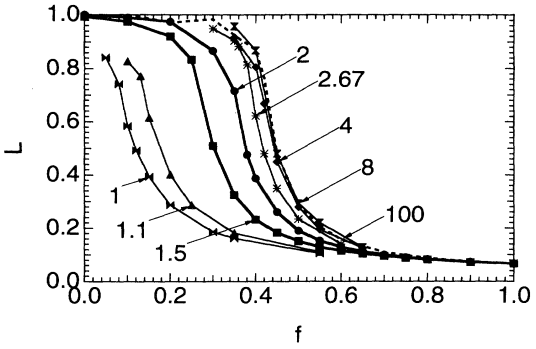

FIG. 2. The steady-state LRO parameter L as a function of f at various temperatures. Each curve is marked with its value of V/kT.

by examining the inflection points of the curves, or by matching values of L to those on the curve for $f=0$, critical values of f for the ordering transition, denoted f_c, were determined. For example, for $V/kT=1.5$ and 2, $f_c=0.275$ and 0.355, respectively. Figure 2 shows that with reduced temperature, the curves of L vs f shift towards the right on Fig. 2, and converge toward the curve for $V/kT=100$. Accordingly, the critical fraction of ballistic atom movements f_c increases and approaches an ultimate limit f_c^0, as discussed below.

For ordered alloys at low values of T and f, there still remains the question of whether the ordered domains tend towards infinite length. This question cannot be answered rigorously with Monte Carlo simulations on finite systems, but we did perform some tests by extrapolation. The characteristic length of ordered domains, $\langle r \rangle$, was calculated as described in Sec. II, and Fig. 3(a) presents typical data on $\langle r \rangle$, in units of the lattice constant, as a function of f at temperatures above T_c^f (or equivalently, for $f>f_c$). The two curves of $\langle r \rangle$ vs f were obtained at fixed temperature, and so are labeled with their individual value of V/kT. As f approaches f_c

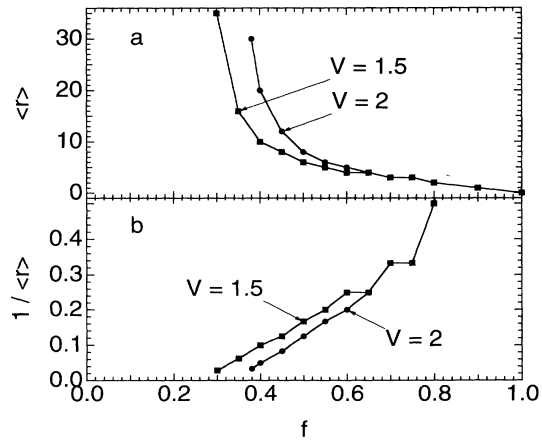

FIG. 3. (a) The steady-state average domain length scale $\langle r \rangle$, and (b) its reciprocal $1/\langle r \rangle$ as functions of f at $V=1.5$ (squares) and $V=2$ (circles), respectively.

from above, $\langle r \rangle$ increases rapidly and approaches a size comparable to the size of the lattice in the simulation. With analogy to a thermodynamic alloy, we might expect $1/\langle r \rangle$ to decrease linearly with $-f$ as f approaches f_c. Figure 3(b) presents curves of $1/\langle r \rangle$ vs f corresponding to the curves in Fig. 3(a). The plateaus at $1/\langle r \rangle = 0.33$ and 0.25 correspond to integral changes in $\langle r \rangle$ from 3 to 4, and are not significant. For larger $\langle r \rangle$, however, there seems to be a linear decrease of $1/\langle r \rangle$ as f approaches f_c. Extrapolating the linear parts of both curves to $1/\langle r \rangle = 0$ gives $f_c = 0.261$ and 0.338 for $V/kT = 1.5$ and 2, respectively. These values are reasonably close to those obtained from the curves of L vs f in Fig. 2.

We compared the dynamical critical temperatures, T_c^f, that were determined from the data of L vs V and from the data of L vs f. The values of f_c from all curves in Fig. 2 are presented as solid circles in Fig. 4. The left axis of Fig. 4 is temperature, normalized by the thermodynamic critical temperature T_c^0 of Eq. (2). Also presented in Fig. 4 as open squares are some results from data of L vs V. These two sets of data are in excellent agreement. Figure 4 is the T-f phase diagram for the steady states of our driven alloy. The solid curve separates the regions of ordered and disordered phases. At $f = 0$, the dynamical phase diagram provides the thermodynamic critical temperature of Eq. (2). The ordered phase is stable for small values of T and f, whereas the disordered phase is stable for large values of T and f. Slightly below the phase boundary, the LRO is imperfect. Slightly above the phase boundary, there is significant SRO. This is typical of a second-order phase transition, and the continuous curves of Figs. 1 and 2 do imply that the transition is of second order for all f.

The nearly linear part of the phase boundary in Fig. 4, between $f = 0$ and $f = 0.36$, was fit to a straight line with a slope of -1.58 ± 0.01:

$$T_c^f = (1 - 1.58f) T_c^0 . \tag{11}$$

As f increased beyond this nearly linear region, T_c^f decreased dramatically. At $f = 0.43$, $T_c^f = 0.01\ T_c^0$. A logarithmic extrapolation to zero temperature of the dashed curve in Fig. 4 provides an ultimate fraction of ballistic atom movements, $f_c^0 = 0.43$, beyond which ordering does not occur at any temperature.

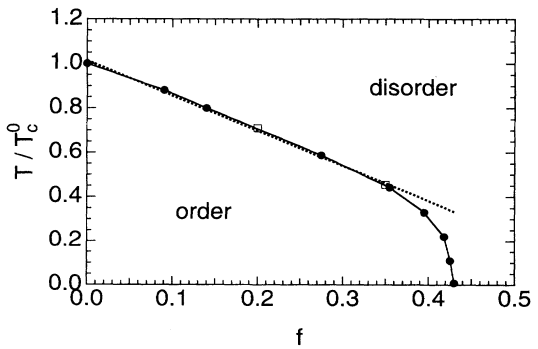

FIG. 4. The T-f dynamical phase diagram for the ordering transition for symmetrical interatomic potentials ($V_{AA} = V_{BB}$). The phase boundary (solid curve) consists of the data points for T_c^f as a function of f. Circles were obtained from simulations with variable f at fixed V, while squares were from simulations with variable V at fixed f. The straight dashed line is a best fit to the linear part of the data.

IV. STEADY STATES WITH BALLISTIC AND THERMAL MOVEMENTS

Here we develop a simple but general analytical theory for the steady state of an ordering alloy in the presence of both ballistic and thermal atom movements. The approach is similar to that of Martin.[21] We use Onsager-type kinetic rate equations, suitably modified to include ballistic atom movements. Onsager-type kinetic rate equations allow us to neglect the details of atom movement mechanisms, thereby simplifying the problem. Nevertheless, this approach should be valid near the steady state of the alloy when dL/dt is zero or nearly zero, which is our present interest for interpreting phase boundaries. We write the time dependence of the LRO parameter for the thermodynamic alloy ($f = 0$) as

$$\frac{dL}{dt} = \frac{l}{kT}\frac{\partial F}{\partial L} , \tag{12}$$

or equivalently,

$$\frac{dL}{dt} = -\frac{l}{kT}\frac{\partial E}{\partial L} + \frac{l}{k}\frac{\partial S}{\partial L} , \tag{13}$$

where l is the mobility coefficient. F and E denote the Helmhotz free energy and enthalpy, respectively. At steady states, L does not change with time. Therefore,

$$T\frac{\partial S}{\partial L} = \frac{\partial E}{\partial L} . \tag{14}$$

In a mean-field thermodynamic calculation ($f = 0$), the contributions to $\partial F/\partial L$ are

$$\frac{\partial E}{\partial L} = \frac{N}{2} zLV , \tag{15}$$

and

$$T\frac{\partial S}{\partial L} = Tk\frac{N}{2}\ln\frac{1-L}{1+L} . \tag{16}$$

It is straightforward to take the mean-field thermodynamic expressions of Eqs. (15) and (16), substitute them into Eq. (14), and recover the mean-field critical temperature $T_c'^0$ of Eq. (3).

For a driven alloy having a fraction of ballistic atom movements, f, the fraction of thermal atom movements is $1-f$. For the thermal atom movements alone, Eq. (13) becomes

$$\left(\frac{dL}{dt}\right)_{\text{thermal}} = -\frac{l}{k}(1-f)\left[\frac{1}{T}\frac{\partial E}{\partial L} - \frac{\partial S}{\partial L}\right] . \tag{17}$$

Because the random ballistic atom movements are assumed to occur at infinite temperature, we have

$$\left(\frac{dL}{dt}\right)_{\text{ballistic}} = -\frac{l'}{k} f\left[\frac{1}{\infty}\frac{\partial E}{\partial L} - \frac{\partial S}{\partial L}\right] , \tag{18}$$

or

$$\left(\frac{dL}{dt}\right)_{\text{ballistic}} = \frac{l'}{k} f \frac{\partial S}{\partial L} \tag{19}$$

for the ballistic atom movements. Equation (19) is an entropy contribution. The enthalpy contribution is zero because the ballistic atom movements are independent of temperature and local environment.

It is important to note that the Onsager mobility constants in Eqs. (13) and (19) are different. As discussed in Sec. V, we expect the thermal atom movements to be increasingly correlated at low temperatures, whereas the ballistic atom movements are not. We define ζ as the ratio of mobility coefficients for the ballistic and thermal atom movements:

$$\zeta \equiv \frac{l'}{l} . \tag{20}$$

It was found in a previous study with the vacancy mechanism that the atom mobility was enhanced by ballistic atom movements,[17] so we expect $l' > l$ and $\zeta > 1$.

Combining Eqs. (17), (19), and (20), we write a complete kinetic equation for the driven alloy:

$$\frac{dL}{dt} = -\frac{l}{kT}(1-f)\frac{\partial E}{\partial L} + \frac{l}{k}[1+(\zeta-1)f]\frac{\partial S}{\partial L} . \tag{21}$$

To obtain the steady-state value of L as a function of T and f, we set Eq. (21) equal to zero and obtain:

$$T\frac{1+(\zeta-1)f}{1-f}\frac{\partial S}{\partial L} = \frac{\partial E}{\partial L} . \tag{22}$$

Consider first the case when $\zeta = 1$, that is, the ballistic atom movements have the same mobility as the thermal atom movements. In this case Eq. (22) becomes

$$\frac{T}{1-f}\frac{\partial S}{\partial L} = \frac{\partial E}{\partial L} . \tag{23}$$

Upon comparison to Eq. (14), we see that the effective temperature, T^{ef}, of the driven alloy is rescaled with respect to the thermal temperature, T:

$$T^{\text{ef}} = \frac{T}{1-f} . \tag{24}$$

Were Eq. (24) true, the dynamical critical temperature of ordering, T_c^f, would decrease linearly with the fraction of ballistic atom movements by simple dilution, becoming zero when $f = 1$:

$$T_c^f = (1-f)T_c^0 . \tag{25}$$

This rescaling of temperature is a consequence of the ballistic atom movements being insensitive to the enthalpy driving force [Eq. (19)]. This reduction of T_c^f by a factor of $1-f$ can be regarded as a dilution of the enthalpy driving force in the presence of the fraction, f, of ballistic atom movements.

In general, however, mobility differences must be considered, and this provides a second means for the ballistic jumps to affect T_c^f. We expect $\zeta \neq 1$, and in fact ζ may be a function of T, f and L. From Eq. (22) we write

$$T^{\text{ef}} = T\frac{1+(\zeta-1)f}{1-f} , \tag{26}$$

and

$$T_c^f = \frac{1-f}{1+(\zeta-1)f}T_c^0 . \tag{27}$$

There is no simple scaling of the critical temperature with f unless $\zeta(T,f,L)$ has a simple form. A precise estimate of ζ is not trivial, and we have not attempted to do so. On the other hand, we have used our Monte Carlo results for T_c^f (Fig. 4) to determine ζ.

V. DISCUSSION

The analysis of Sec. IV relies on a single order parameter L to characterize the microstructures of the driven alloy. It is appropriate to ask if a single LRO parameter is adequate to characterize the microstructures of the driven alloys, or if the steady-state microstructures of alloys having the same value of L, but subjected to different combinations of T and f may have different order parameters on short length scales. To address this concern, we compared both the LRO and SRO parameters for the steady states of alloys with various combinations of T and f. Figure 5 shows steady-state values of the SRO parameters $\alpha(1)$ and $\alpha(2)$ as functions of L for alloys with various combinations of T and f. The curves are nearly identical. Direct observation of the alloys also confirmed that alloys with the same steady-state values of L were very similar in appearance. The LRO parameter L seems a reasonable single parameter for specifying the steady state of order in our driven alloys.

We now use the analytical approach of Sec. IV with its Onsager-type kinetic rate equation for L to interpret the Monte Carlo results of Fig. 4. For $f \leq 0.36$ or $V/kT \leq 2$, Eq. (11) describes our data well. By comparing Eqs. (11) and (27), we obtain

$$\zeta \equiv \frac{l'}{l} = \frac{1.58(1-f)}{1-1.58f} . \tag{28}$$

According to Eq. (28), the mobility ratio ζ increases

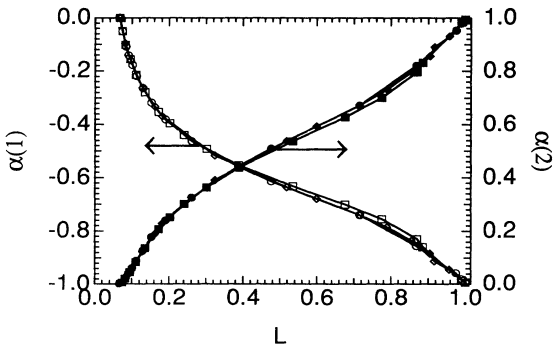

FIG. 5. SRO parameters, $\alpha(1)$ and $\alpha(2)$, vs LRO parameter, L, for steady states of several alloys. $\alpha(1)$: open marks against the left axis; $\alpha(2)$: solid marks against the right axis. Squares: thermodynamic alloys ($f = 0$) at various T; diamonds: driven alloys at various T with fixed $f = 0.35$; circles: driven alloys with various f at fixed $V/kT = 2$.

slightly as f increases. A much more dramatic increase in ζ occurs when $f>0.36$ or $V/kT>2$. These increases in ζ are not surprising for ordered alloys, however. At low temperatures (corresponding to large f on the phase boundary of Fig. 4) thermal diffusion in ordered alloys becomes highly correlated and inefficient, effectively suppressing l. For thermodynamic ordering transitions on a square lattice, there are dramatic changes in vacancy mobility when $V/kT>2$.[14] At these low temperatures, the vacancy becomes trapped in local regions from which it has insufficient thermal activation for escape. We found the same type of vacancy trapping in the present study. At the lowest temperatures, the vacancy moved cyclically between a set of sites until it was dislodged by a ballistic atom movement. This high degree of diffusional correlation suppresses strongly the effective thermal mobility coefficient l. On the other hand, we do not expect the mobility coefficient for ballistic atom movements l to change with temperature. We therefore expect the mobility ratio ζ to increase with decreasing temperature, suppressing T_c^f dramatically when $V/kT>2$.

To investigate further these effects of vacancy mobility, we performed some Monte Carlo simulations with asymmetrical chemical interaction potentials between A and B atoms ($V_{AA}\neq V_{BB}$), while maintaining the same thermodynamic pair exchange potential V. It was established previously that diffusion coefficients, and therefore the effective mobility constants, will change when $V_{AA}\neq V_{BB}$.[14] Figure 6 shows typical L vs f curves for the same thermodynamic potential, $V=2$, but for two different cases, one with $V_{AA}=V_{BB}$, and the other with $V_{AA}\neq V_{BB}$. Although the shapes of the curves are similar, the critical values of f are quite different: $f_c=0.20$ for the asymmetrical case, while $f_c=0.35$ for the symmetrical case. This cannot be a thermodynamic effect, since Eqs. (2) and (3) depend only on V. The symmetry of the interatomic potentials must affect f_c through the mobility coefficients. Correlated thermal vacancy motion can explain this behavior. Vacancy trapping is controlled by the strongest interatomic potential,[14] so in the approximately linear region of Fig. 4, we expect f_c to decrease by the factor of $\frac{2}{3}$ as V_{AA} increases from 2 to 3. This is approximately correct.

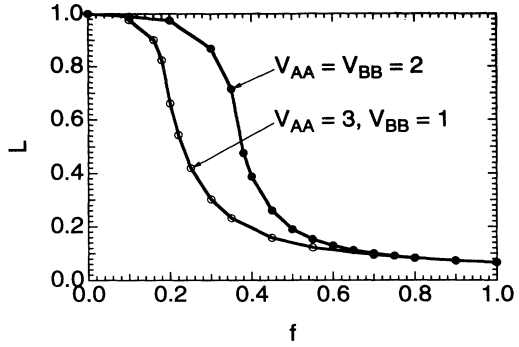

FIG. 6. The steady-state LRO parameter, L, as a function of f for alloys with the same thermodynamic exchange potential, $V=2$. Solid circles: symmetrical case with $V_{AA}=V_{BB}=2$. Open circles: asymmetrical case with $V_{AA}=3$ and $V_{BB}=1$.

VI. SUMMARY

We performed a Monte Carlo study of steady states in alloys with thermal and ballistic atom movements. A vacancy mechanism was used for atom movements in equiatomic alloys on a square lattice. A T-f phase diagram for the order-disorder transition was constructed for alloys with symmetical interatomic potentials ($V_{AA}=V_{BB}$). When $f<0.36$, the dynamical critical temperature decreased by the factor $1-1.58f$ in the presence of a fraction of ballistic atom movements f. For f greater than 0.36, but less than 0.43, the reduction of the critical temperature with f was much more rapid, and the critical temperature became zero at a critical value of f, $f_c^0=0.43$. An Onsager-type analytical theory was used to explain this behavior. The decrease in critical temperature with f occured for two reasons. First, in the presence of ballistic atom movements, the enthalpy driving force for ordering, $-\partial E/\partial L$, is diluted by the factor $(1-f)$. Second, the mobility coefficient for thermal atom movements becomes small at low temperatures, owing to a high degree of correlation in the vacancy diffusion mechanism. The ballistic atom movements are not subject to this correlation factor, and so are relatively more important at low temperatures, leading to a dramatic drop of T_c to zero near $f=0.43$.

ACKNOWLEDGMENTS

We thank Professor W. L. Johnson and Dr. L. Anthony for useful discussions. This work was supported by NSF under Contract No. DMR-9213447.

[1]See, for example, C. C. Koch, O. B. Kalvin, C. G. McKamey, and J. O. Scarbrough, Appl. Phys. Lett. **43**, 1017 (1983); R. B. Schwarz, R. Petrich, and C. Saw, J. Non-Cryst. Solids **76**, 281 (1985); J. Eckert, J. C. Holzer, C. E. Krill, III, and W. L. Johnson, J. Appl. Phys. **73**, 2794 (1993).

[2]See, for example, K. C. Russell, Prog. Mater. Sci. **18**, 229 (1984); J. S. Williams, R. G. Elliman, W. L. Brown, and T. E. Seidel, Phys. Rev. Lett. **55**, 1482 (1985); H. A. Atwater, C. V. Thompson, and H. I. Smith, *ibid.* **60**, 112 (1988).

[3]W. Feller, *An Introduction to Probability Theory and Its Applications* (Wiley, New York, 1957), Vol. 1, Chap. 15.

[4]P. Bellon and G. Martin, Phys. Rev. B **38**, 2570 (1988).

[5]P. Bellon and G. Martin, Phys. Rev. B **39**, 2403 (1989).

[6]G. Martin, Phys. Rev. B **41**, 2279 (1990).

[7]F. Haider, P. Bellon, and G. Martin, Phys. Rev. B **42**, 8274 (1990).

[8]E. Salomons, P. Bellon, F. Soisson, and G. Martin, Phys. Rev. B **45**, 4582 (1992).
[9]P. Bellon, Phys. Rev. B **45**, 7517 (1992).
[10]P. Bellon, F. Soisson, and G. Martin, in *Diffusion in Ordered Alloys,* edited by B. Fultz, R. W. Cahn, and D. Gupta (TMS, Chicago, 1992).
[11]F. Haider, in *Ordering and Disordering in Alloys,* edited by A. R. Yavari (Elsevier, Amsterdam, 1992).
[12]J. R. Beeler, Jr. and J. A. Delaney, Phys. Rev. **130**, 962 (1963).
[13]J. R. Beeler, Jr., Phys. Rev. A **138**, 1259 (1965).
[14]B. Fultz, J. Chem. Phys. **87**, 1604 (1987).
[15]B. Fultz, J. Chem. Phys. **88**, 3227 (1988).
[16]H. Ouyang and B. Fultz, J. Appl. Phys. **66**, 4752 (1989).
[17]L. B. Hong, L. Anthony, and B. Fultz, J. Mater. Res. (to be published).
[18]L. Onsager, Phys. Rev. **65**, 117 (1944).
[19]B. E. Warren, *X-Ray Diffraction* (Addision-Wesley, Reading, MA, 1969), Chap. 12.
[20]L. Anthony and B. Fultz, J. Mater. Res. **9**, 348 (1994).
[21]G. Martin, Phys. Rev. B **30**, 1424 (1984).